

Manipulating Cherenkov Radiation and Smith–Purcell Radiation by Artificial Structures

Zhaoxian Su, Bo Xiong, Yihao Xu, Ziqiang Cai, Jianbo Yin, Ruwen Peng, and Yongmin Liu*

A moving charged particle, such as an electron, can radiate light due to the interaction between its Coulomb field and surrounding matter. This phenomenon has spawned great interest in the fields of physics, electron microscopy, optics, biology, and materials science. Since the radiation generated by the charged particles strongly depends on the surrounding matter, artificially engineered materials with exotic electromagnetic and optic properties, including metamaterials and metasurfaces, provide an unprecedented opportunity to tailor the interaction between the charged particle and matter, and ultimately enable to manipulate the radiated light. In this review, the fundamentals of Cherenkov radiation and Smith–Purcell radiation are presented. Subsequently, the recent advances in the control of Cherenkov radiation and Smith–Purcell radiation based on metamaterials and metasurfaces are summarized. Finally, the applications using these two physical phenomena, including electron-driven photon sources and electron accelerators, are discussed in this review.

1. Introduction

It has been decades since people discovered that electrons and other charged particles can lead to far-field radiation. When a charged particle moves in a medium, the medium will polarize under its dynamically changing Coulomb fields and become

a radiation source, producing coherent radiation.^[1,2] The radiation can be induced by different physical mechanisms, all of which can be well explained by Maxwell's equations. The most widely known radiations include transition radiation,^[3,4] Cherenkov radiation,^[5] and diffraction radiation.^[6] The transition radiation occurs as a moving electron impinges on the interface of two materials due to the annihilation of its image. If an electron moves with a velocity greater than the phase velocity of light in the surrounding medium, the interaction between the electron and surrounding medium leads to Cherenkov radiation. As for the diffraction radiation, it happens when the moving electron is near a structured surface. The most typical diffraction radiation is Smith–Purcell radiation,^[7,8] which occurs

when electrons move closely parallel to a periodic grating. The radiated light depends on not only the electron beam but also the surrounding medium. Investigating the interaction between electrons and surrounding matter has attracted extensive attention due to its importance in the fields of electron microscopy, particle physics, medical imaging, and therapy.^[9]


Recently, metamaterials have become one research frontier in science and technology. Metamaterials are novel materials which comprise metallic or dielectric structures with the size and spacing much smaller than the wavelength of interest. These structured elements, acting as man-made “atoms,” can regulate the interactions between metamaterials and external electromagnetic waves, including light waves.^[10–13] Enabled by metamaterials, a multitude of novel material properties and applications have been demonstrated, which include negative,^[14,15] zero^[16,17] or extremely large refractive indices,^[18,19] strong anisotropy,^[20,21] broadband chirality,^[22–25] large nonlinearity,^[26–28] sub-diffraction-limited imaging,^[29–31] and invisibility cloak.^[32–36] Since 2012, there has been an extensive interest in 2D metamaterials, known as metasurfaces, with thickness of only a few tens of nanometers.^[37–51] By tailoring the geometry of the building blocks of a metasurface and engineering their spatial distribution, we can control the amplitude, polarization state, phase, as well as the trajectory of light on an entirely planar platform. With structured metamaterials and metasurfaces, we have new degrees of freedom to tailor the interaction between the electrons and surrounding matter. On one hand, it is fundamentally interesting to explore how electrons interact

Z. Su, B. Xiong, Y. Xu, Prof. Y. Liu
Department of Mechanical and Industrial Engineering
Northeastern University
Boston, MA 02115, USA
E-mail: y.liu@northeastern.edu

B. Xiong, Prof. R. Peng
National Laboratory of Solid State Microstructures
School of Physics
Collaborative Innovation Center of Advanced Microstructures
Nanjing University
Nanjing 210093, China

Z. Cai, Prof. Y. Liu
Department of Electrical and Computer Engineering
Northeastern University
Boston, MA 02115, USA

Z. Su, Prof. J. Yin
Smart Materials Laboratory
Department of Applied Physics
Northwestern Polytechnical University
Xi'an 710129, China

 The ORCID identification number(s) for the author(s) of this article can be found under <https://doi.org/10.1002/adom.201801666>.

DOI: 10.1002/adom.201801666

with artificial meta-atoms and then radiate light, so that we can go beyond the scenario in which conventional light–matter processes are concerned. On the other hand, metamaterials and metasurfaces can drastically influence the characteristics of the radiated light, opening a new paradigm to control electron-induced emission. Indeed, we have witnessed exciting breakthroughs in this area over the past years, and it is time to review the progress and provide some outlooks.

The rest of the review is organized as follows: First, we will give a general introduction to Cherenkov radiation and Smith–Purcell radiation in Section 2. We will briefly explain the physical mechanisms of the two kinds of radiations and show the connection and difference between them. In Section 3, we will present the control of Cherenkov radiation using artificial structures. The properties of the Cherenkov radiation, including the radiation direction and the generation condition, can be easily changed by the surrounding artificial materials. Section 4 will focus on Smith–Purcell radiation manipulated by artificially structured materials, showing that the intensity, spatial distribution, and the polarization of the Smith–Purcell radiation can all be tailored by structured materials. Then we will discuss the applications of Cherenkov radiation and Smith–Purcell radiation, followed by the conclusion and outlook.

2. Background of Cherenkov Radiation and Smith–Purcell Radiation

In 1934, Cherenkov observed visible light emission from clear liquids exposed to gamma rays, which was later named Cherenkov radiation.^[51] This phenomenon was theoretically explained by Tamm and Frank in 1937.^[52] The three scientists shared the Nobel prize in physics in 1958 for the discovery and the interpretation of the Cherenkov effect. The underlying mechanism of Cherenkov radiation can be explained as follows: when a charged particle moves in a homogeneous medium, electric dipoles will be induced in the medium through the Coulomb field of the particle. If the speed of the charged particle is higher than the phase velocity of light in the medium, the induced electric dipoles could become the source and radiate with coherent wavefronts as described by Huygens's principle.^[53] As schematically shown in **Figure 1a**, the charged particle with a velocity v moves after a given time t from the

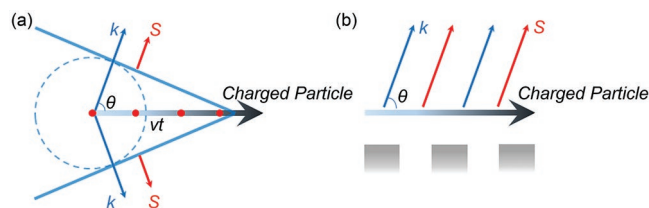


Figure 1. a) Schematic of Cherenkov radiation. The red dots represent a charged particle moving in a dielectric medium. The blue arrows and red arrows indicate the direction of the wavevector k and Poynting vector S of the emitted wave, respectively. The wave front propagates forward at an angle θ with respect to the direction of the moving particle. b) Schematic of Smith–Purcell radiation, in which the evanescent wave generated by a charged particle can be coupled out to the far field by a periodic grating.



Jianbo Yin is a professor at Department of Applied Physics, Northwestern Polytechnical University, China. He obtained his B.E. in chemical engineering in 1998 and Ph.D. in materials physics and chemistry in 2010 from Northwestern Polytechnical University. Then, he joined Smart Materials Lab at the same university working on smart fluids. He has published over 100 peer-reviewed papers (including 25 papers in Chinese), 15 Chinese patents, three book chapters, and one book. His present research focuses on smart electrorheological and magnetorheological fluids, tunable metamaterials and metasurfaces.



Ruwen Peng received her Ph.D. in condensed matter physics from Nanjing University, China in 1998. Currently she is a distinguished professor in Nanjing University and a principal investigator at National Laboratory of Solid State Microstructures (NLSSMs) in Nanjing University. Her current research interests include plasmonics and nanophotonics, metamaterials, photonic quasicrystals, phononic transport, and heat transfer in nanostructures.



Yongmin Liu obtained his Ph.D. from the University of California, Berkeley in 2009. He joined the faculty of Northeastern University at Boston in fall 2012 and is currently an associate professor in the Department of Mechanical & Industrial Engineering and the Department of Electrical & Computer Engineering. His research interests include nano-optics, nanoscale materials, plasmonics, metamaterials, and nano-optomechanics. He has authored and coauthored more than 80 journal papers. He was a recipient of NSF CAREER Award (2017), ONR Young Investigator Award (2016), and 3M Non-Tenured Faculty Award (2016).

initial moment, leading to a shock wave nearby the particle. In the given time, the distance that the particle moves is vt , while the distance that the emitted wave travels is ct/n , where n is the refractive index of the surrounding medium at frequency ω and v is the speed of the light in vacuum. As a result, the well-known relation of the angle between Cherenkov radiation and the direction of moving particle can be derived as

$$\cos \theta = \frac{c}{nv} \quad (1)$$

From Equation (1), we find Cherenkov radiation can occur in a conventional medium with a positive refractive index when the condition $v > c/n(\omega)$ is met. The direction of the radiated wave is determined by not only the velocity of the particle but also the refractive index of the surrounding medium. Meanwhile, the energy of radiated wave per unit frequency per distance travelled by the particle can be described by the Frank–Tamm formula^[52]

$$\frac{d^2E}{dx d\omega} = \frac{q^2}{4\pi} \mu \omega \left(1 - \frac{c^2}{v^2 n^2} \right) \quad (2)$$

where μ is the frequency dependent permeability and q is the electric charge of the particle. From Equation (2), one can see that the radiated power is also related to the electromagnetic property of the surrounding medium. The traditional equations describing the Cherenkov radiation need to be revisited when metamaterials are involved, because the effective electromagnetic properties of metamaterials can be strongly dispersive and extraordinary. Thanks to the unique properties of metamaterials, we can steer the Cherenkov radiation direction, lower the energy threshold of the particle for Cherenkov radiation, and enhance the radiation efficiency. We will discuss these novel effects in Section 3 in detail.

If the velocity of moving charged particles is lower than the phase velocity of light in the surrounding medium, electromagnetic fields associated with the charged particle are nonradiative. A periodic grating can provide Bloch wavevectors to couple the bound energy into the far field (Figure 1b), giving rise to Smith–Purcell radiation that was discovered by Smith and Purcell in 1953.^[7] The relation between the radiation wavelength and the particle velocity can be described as

$$\lambda_0 = \frac{p}{|m|} \left(\frac{c}{v} - \cos \theta \right) \quad (3)$$

where λ_0 is the wavelength of the radiation wave, p is the period of the grating, m is the diffraction order, θ is the angle between the moving particle and radiation wave. Van den Berg calculated the incoherent Smith–Purcell radiation from an electron moving above an infinitely long grating.^[54–56] About 20 years later, coherent Smith–Purcell radiation was observed by using bunched electrons.^[57,58] For electrons that are bunched into a small region compared to the radiation wavelength, the radiation from each electron is in phase and the radiated electromagnetic fields can be superimposed. For coherent Smith–Purcell radiation, the radiated energy can be increased quadratically with the number of electrons in the bunch. If Smith–Purcell radiation is induced by the periodic repeated electron bunches,

the radiation intensity will be enhanced at the frequency of the bunches and its harmonics. This phenomenon is called super-radiant emission of Smith–Purcell radiation.^[59–61]

Compared to Cherenkov radiation that occurs within the medium, Smith–Purcell radiation is generated by a periodic grating but then propagates in a uniform medium. However, just as Cherenkov radiation, Smith–Purcell radiation also depends on the surrounding medium. Up to now, many structures have been proposed and explored to manipulate Smith–Purcell radiation, including the intensity, spatial distribution, and the polarization state, which will be discussed in Section 4.

3. Manipulating Cherenkov Radiation by Metamaterials

3.1. Reversed Cherenkov Radiation and Steering Cherenkov Light

In 1968, Viktor hypothesized a material with simultaneously negative permittivity and permeability.^[62] It was found that the wave vector \mathbf{k} , electric field vector \mathbf{E} , and magnetic field vector \mathbf{H} of a plane wave propagating in such a medium follow the left-hand rule, and the resulting refractive index is negative. Therefore, this kind of materials can be called left-handed materials or negative-index materials (NIMs). In order to achieve NIMs, electric permittivity and magnetic permeability need to be negative simultaneously. In his seminal paper, Viktor predicted many peculiar properties associated with NIMs, such as negative refraction of light, reversed Doppler effect, as well as reversed Cherenkov radiation. More specifically, the angle between the moving particle and Cherenkov radiation, which forms the Cherenkov emission cone, is limited within the range from 0° to 90° in a dielectric medium with a positive refractive index (Figure 1a). However, in a negative-index material, the Cherenkov radiation is flipped toward the backward direction, and the angle of radiation cone becomes obtuse. In other words, the transverse component of wave vector is directed toward the moving particles, while the energy flows away from the moving particles to infinity,^[63,64] as shown in Figure 2a. The reversed Cherenkov radiation is expected to reduce the interference and lead to more accurate Cherenkov detectors.

Reversed Cherenkov radiation in an NIM was only investigated in theory and simulation at the early stage.^[65,66] With the rapid development in the design, fabrication, and characterization of metamaterials, low-loss NIMs became available for researchers to experimentally demonstrate reversed Cherenkov radiation. The first experiment was conducted in the frequency range from 8.1 to 9.5 GHz.^[67] As shown in Figure 2b, the unit cell of the NIM contains structured copper strips on both sides of a polytetrafluoroethylene substrate. To realize a reversed Cherenkov radiation, a metamaterial structure was designed to possess negative permittivity in the x – z plane and negative permeability along the y -direction, which were provided by two orthogonal straight copper wires and L-shaped metal strips, respectively. From the refraction measurements on a prism-shaped sample composed by the metamaterial, the authors confirmed that the effective refractive index

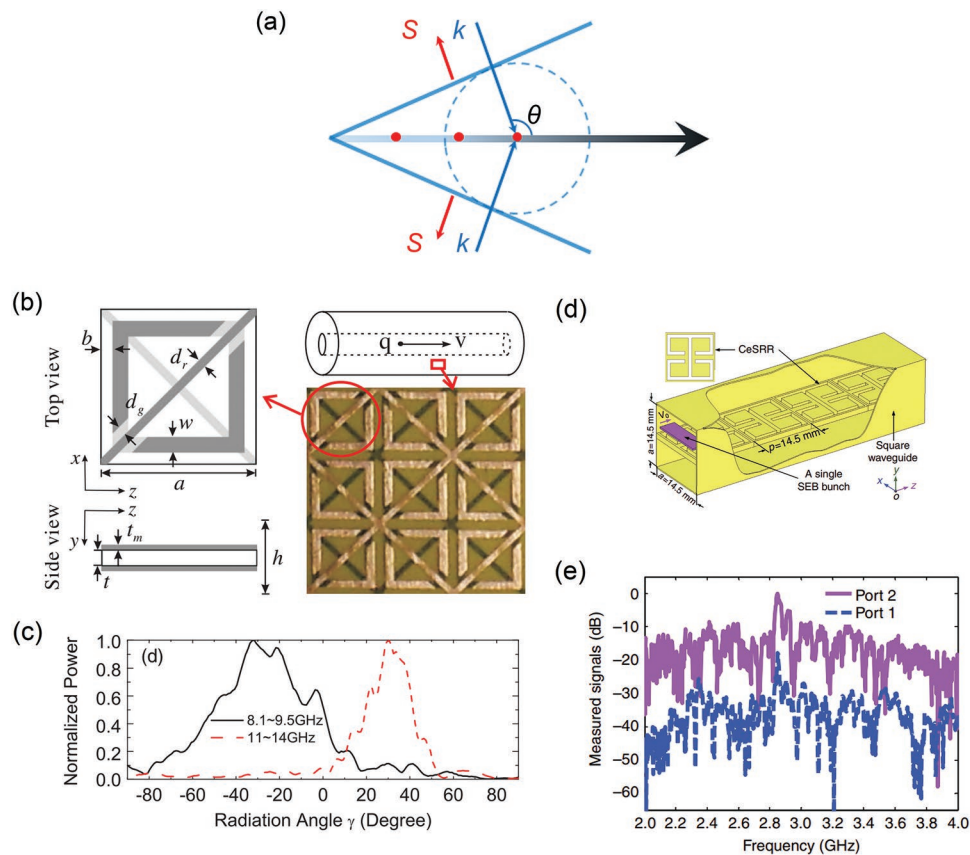


Figure 2. a) Schematic of reversed Cherenkov radiation. In contrast to normal Cherenkov radiation shown in Figure 1a, the radiation angle θ becomes obtuse. b) Illustration (left panel) and photograph (right panel) of the NIM medium. c) Spectra of the radiation power at different radiation angles for the negative band (black solid line) and positive band (red dashed line). d) Schematic diagram of the constructed structure interacting with a single sheet electron beam bunch travelling along the $+z$ direction. e) The measured power spectral densities of microwave signals at ports 2 and 1, when the electron beam moved from port 2 to port 1. The peak power at 2.847 GHz at port 1 is 17.6 dB, lower than the 2.850 GHz RCR at port 2. (b),(c) Reproduced with permission.^[67] Copyright 2009, American Physical Society. (d),(e) Reproduced with permission.^[68] Copyright 2017, Nature Publishing Group.

is negative from 8.1 to 9.5 GHz. By using a phased dipole array to imitate the behavior of a moving charged particle, they measured the angular distribution of radiation power. As shown in Figure 2c, the radiation power in the negative band points toward the backward direction, confirming the existence of reversed Cherenkov radiation.

Duan et al. reported the experimental work by using real charged particles to generate Cherenkov radiation in an NIM. The NIM consists of a square waveguide loaded with complementary electric split ring resonators (CeSRRs), as shown in Figure 2d.^[68] The CeSRR layer can provide negative permittivity along the x -direction. The hollow square waveguide can be regarded a 1D lossless magnetic plasma with negative permeability, because the TM_{11} waveguide mode is below the cut-off frequency. As a result, the metamaterial shows negative index from 2.83 to 3.05 GHz. In the experiment, the author applied two couplers at the ends of the waveguide to measure the radiated power. The graphite cathode and graphite collector were used to produce a single sheet electron beam bunch and collect the residual electrons from the bunch, respectively. The electron beam moved from port 2 to port 1. However, much higher radiated power was observed in port 2, which is in the opposite direction to the movement of the electron beam bunch (Figure 2e).

From Equation (1), we can see that the angle of Cherenkov cone in a nonmagnetic material depends on the particle velocity and the permittivity of the material. When the particle velocity is very high, Equation (1) approaches 0 for a conventional dielectric medium. As a result, the angle of the Cherenkov cone saturates to a value independent of the velocity of the particle. In this case, anisotropic metamaterials based on transformation optics can be used to present the Cherenkov angle of different particle velocity.^[69] In this work, the authors applied a linear coordinate stretching along the principle axes to transform the permittivity of background medium, so that the radiation angle in the electromagnetic space can be transformed into the angle in the physical space. The proposed metamaterial corresponds to silver cylinders embedded in a dielectric matrix. However, the loss of the metal-based systems will make the relation between the Cherenkov angle and the particle velocity distorted and broadened. To overcome the influence of the loss in the anisotropic metal-based metamaterial with complex permittivity, Lin et al. proposed a new mechanism of effective Cherenkov radiation generated by the constructive interference of resonance transition radiation excited in alternating two different dielectric materials (Figure 3a).^[70] When the resonance transition radiation interferes constructively

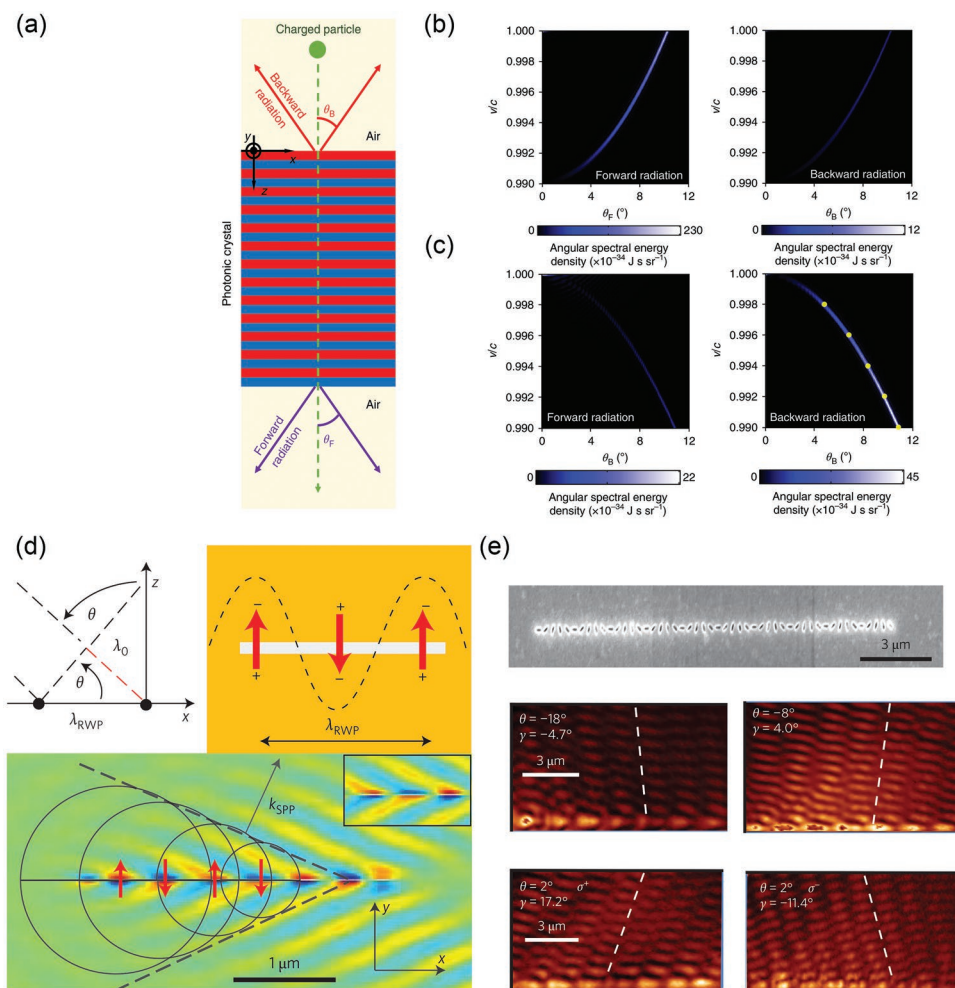


Figure 3. a) Scheme of the layered structure for changing the radiation angle of Cherenkov radiation. Red region and blue region correspond to different dielectric layers. The forward (backward) radiation is collected in the bottom (top) air region. b) and c) Calculated angular spectral energy density of forward and backward radiation for two different photonic crystals. In (b) $d_{\text{unit}} = 1.0205\lambda$, $d_1 = 0.3d_{\text{unit}}$, $d_2 = 0.7d_{\text{unit}}$ and in (c) $d_{\text{unit}} = 0.2792\lambda$, $d_1 = 0.6d_{\text{unit}}$, $d_2 = 0.4d_{\text{unit}}$. The yellow dots in (c) denote Cherenkov angles at five different particle velocities. d) Top: Schematic of the generation of the RWP of wavelength λ_{RWP} when light impinges on a slit in a metal film at oblique incidence θ with free-space wavelength λ_0 . The red dashed line denotes an extra path length of one free-space wavelength, such that the light incident at the black dots has the same phase. Bottom: Simulated out-of-plane field distribution (E_z) of generated surface plasmon wakes. e) Top: Scanning electron micrograph of the nanostructures used to generate the surface plasmon wakes. Middle: NSOM images for different angles of incidence of σ^+ polarized wave. Bottom: NSOM images for incidence of σ^+ polarized wave and σ^- polarized wave. (a)–(c) Reproduced with permission.^[70] Copyright 2018, Nature Publishing Group. (d), (e) Reproduced with permission.^[71] Copyright 2015, Nature Publishing Group.

in air, it can be regarded as the effective Cherenkov radiation that propagates in the form of Bloch modes and can be coupled out to air. However, when the resonance transition radiation interferes destructively in air, the corresponding Bloch modes cannot be coupled out to air and are trapped inside the photonic crystal by total internal reflection. Through this mechanism, both constructive and destructive interference of resonance transition radiation in the forward and backward directions can be realized. Figure 3b,c shows the angular spectral energy density at the working wavelength of 700 nm in the forward and backward directions for two different photonic crystals. For the first photonic crystal, the resonance transition radiation has a constructive interference in the forward direction and a destructive interference in the backward direction. On the contrary, the resonance transition radiation of the

second photonic crystal leads to constructive (destructive) interference in the backward (forward) direction. One can see that the radiation angles of the layered structure are very sensitive to the particle velocity, promising novel detectors for particles with high momentum.

The direction of 2D analogue of Cherenkov radiation can also be controlled by structured materials. Genevet et al. designed a metasurface consisting of 1D subwavelength rotated apertures.^[71] For a S-polarized incident beam, the 1D aperture array can generate a running wave of polarization (RWP) that propagates faster than the phase velocity of surface plasmon polaritons (SPPs), which are optical surface waves supported at a metal–dielectric interface, as Figure 3d shows. The RWP can be regarded as a series of dipoles along the apertures so that it can mimic the moving charged particles. The RWP excites SPPs

that propagate on the metal surface in analogy to Cherenkov radiation, and form wakes at an angle γ . The rotated apertures could induce an additional phase shift along the 1D structure for circular polarized wave, and the angle is given by

$$\sin \gamma = \frac{\sin \theta}{n_{\text{eff}}} + \sigma_{\pm} \frac{1}{k_{\text{spp}}} \frac{\pi}{\Gamma} \quad (4)$$

Here θ is the incident angle, n_{eff} is the effective index of the SPP mode on a metal/air interface defined as $n_{\text{eff}} = \lambda_0/\lambda_{\text{spp}}$, k_{spp} is the wavevector of SPP wakes. Γ is the period of the rotated apertures, and $\sigma_{\pm} = \pm 1$ is the photon's spin, corresponding to right and left circular polarizations, respectively. We can find that the direction of the generated surface plasmon wakes are related to the incident angle and the spin angular momentum of the incident wave. With a near-field scanning optical microscope (NSOM) set-up to excite the apertures with a circularly polarized focused Gaussian beam at oblique incidence, the steering of surface plasmon wakes for different incident angle and different photon spins can be clearly observed. As shown in Figure 3e, the measurements are in excellent agreement with the theoretical expected angles. For the incident wave with the same polarization, we can get forward or reversed SPP wakes by changing the incident angle. Meanwhile, the direction of SPP wakes can be forward or backward by switching the spin of the photon when the incident angles are small.

3.2. Decreasing the Energy Threshold of Cherenkov Radiation

There is a key characteristic of Cherenkov radiation in a conventional material: the velocity of the moving charged particle needs to be higher than the phase velocity of light in the medium. So high-energy electrons are required to generate Cherenkov radiation experimentally, which are difficult to achieve in experiments and make the Cherenkov radiation inaccessible to most nanoscale electronic and photonic devices. People have been seeking innovative ways to reduce or even eliminate the energy threshold of particle, which can substantially improve the performance of free electron lasers based on Cherenkov radiation. In an isotropic material whose permittivity is frequency dependent, Stevens et al. have demonstrated theoretically and experimentally that the subluminal charged particle can lead to Cherenkov radiation below the light threshold through phonon-assisted phase matching.^[72] Artificially structured materials also provide a new method for decreasing the particle energy threshold in Cherenkov radiation. Luo et al. have investigated the Cherenkov radiation in a 2D photonic crystal and demonstrated that the threshold could disappear.^[73] Cherenkov radiation in photonic crystal results from a coherent excitation of eigenmodes of the photonic crystal by the moving charged particles and propagates in the form of Bloch waves. In the photonic crystal, the eigen frequency should match the dispersion relation of Cherenkov radiation when the radiation occurs

$$\omega_n(k) = k \cdot v \quad (5)$$

where the subscript n represents the band index. When Equation (4) is satisfied, the dispersion plane of Cherenkov

radiation mode will intersect with a photonic-crystal dispersion surface. The authors found that Cherenkov radiation depends on different velocity ranges of moving charged particle. In the regime where the particle velocity is far below the long-wavelength phase velocity ($v \ll 0.1c$) of the photonic crystal, the Cherenkov radiation shows the character of Smith–Purcell radiation. In a higher velocity range ($v \approx 0.15c$), the Cherenkov radiation results from the merge of the first and higher Smith–Purcell resonances and the radiation pattern has a backward-pointing overall cone. In the $0.2c < v < 0.4c$ regime, the Cherenkov radiation is backward. The $v > v_c$ regime is the normal regime and the radiation cone is forward.

Cherenkov radiation in anisotropic metallic metamaterial, including metallic wire arrays^[74,75] and metallic layers embedded in a dielectric medium,^[76,77] has also been studied. These metamaterials can be described by an effective permittivity tensor. The radiation wave in these metamaterials propagates along the metallic wire or metallic slab with velocity $c/\sqrt{\epsilon_h}$, whereas the velocity of the moving charges is v . Hence the angle of radiation cone follows the relation $\tan \theta = c/v\sqrt{\epsilon_h}$, where ϵ_h is permittivity of the host medium of the metallic wire or slab. As Figure 4a shows, in the wire medium, the main radiation channel is associated with the quasi-transverse electromagnetic (TEM) mode, whose dispersion depends on $|k_y| = \sqrt{\epsilon_h} \omega/c$. No matter how low the particle velocity is, it is always possible to couple the moving charges to a propagating mode. Theoretical studies have shown that the number of electromagnetic states in the wire medium is roughly proportional to the density of wires. More number of radiative channels can be obtained by increasing the density of wires, leading to the enhancement of the Cherenkov emission. As a result, not only the energy threshold for Cherenkov radiation in these anisotropic metamaterials is significantly suppressed, but the intensity of the radiation is enhanced by several orders compared to the conventional radiation. These intriguing phenomena have stimulated experimental effort. For instance, Liu et al. demonstrated that the electron velocity threshold for Cherenkov radiation in hyperbolic metamaterial can be eliminated.^[78] When the free electrons move on the top of the hyperbolic metamaterial surface, the condition for generating Cherenkov radiation is different from that in conventional media. For type I hyperbolic metamaterial with permittivity $\epsilon_x < 0$ and $\epsilon_z > 0$, Cherenkov radiation has no threshold for the electron bunch velocity. For type II hyperbolic metamaterial with permittivity $\epsilon_x > 0$ and $\epsilon_z < 0$, the Cherenkov radiation can be generated when the condition $v < c/\sqrt{\epsilon_x}$ is met. Liu et al. fabricated a metamaterial composed by Au/SiO₂ multilayers (Figure 4b,c) that can be regarded as type II hyperbolic metamaterial when the wavelength is larger than 425 nm. Upon applying voltage on the Mo electrodes that were integrated on the metamaterial, the emitted electrons could move from the cathode tip to anode. In the experiment, the output power of light result from Cherenkov radiation was much larger than the white noise even though the voltage is as low as 0.25 kV (Figure 4d). Through measuring the output intensity of the sample with different periods of nanoslits, the Cherenkov radiation in a broad wavelength range can be observed (Figure 4e). The region of Cherenkov radiation according to the calculated effective permittivity and particle velocity is shown in Figure 4f.

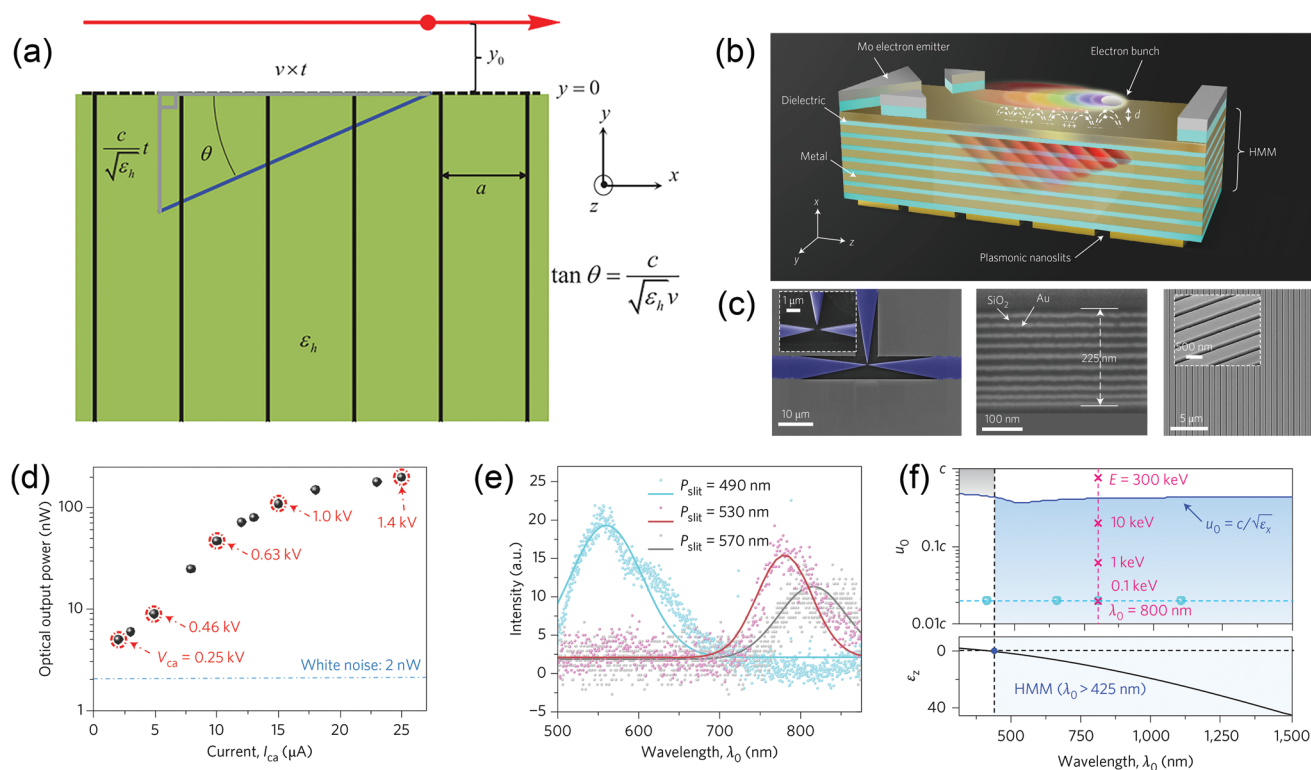


Figure 4. a) Scheme of Cherenkov radiation when a beam of moving charged particle propagates in the vicinity of a wire medium along the x -direction. b) Schematic of the Cherenkov radiation emitter consisting of a planar Mo electron emitter, multilayer hyperbolic metamaterial, and plasmonic periodic nanoslits. c) Scanning electron microscope images of the Cherenkov radiation emitter. Left: planar Mo electron emitter. Middle: hyperbolic metamaterials. Right: periodic Au nanoslits. d) Optical output power for different cathode–anode voltage V_{ca} . e) Spectra of output light with different periods of slits (P_{slit}). Gray, red, and turquoise curves/symbols correspond to $P_{slit} = 570$ nm ($V_{ca} = 1.15$ kV), 530 nm ($V_{ca} = 1.4$ kV), and 490 nm ($V_{ca} = 1.35$ kV), respectively. f) The region for Cherenkov radiation generation in the multilayer metamaterials. Cherenkov radiation can be generated in the blue shaded area and the gray shaded area. (a) Reproduced with permission.^[74] Copyright 2012, American Physical Society. (b)–(f) Reproduced with permission.^[78] Copyright 2017, Nature Publishing Group.

More specifically, Cherenkov radiation covering 500–900 nm can be obtained with an electron energy of only ≈ 0.25 –1.4 keV, which is several orders of magnitude lower than the previous report.^[79] Recently, Kaminer et al. predicted that the threshold of 2D Cherenkov radiation in graphene can be modified by the quantum effect.^[80] Because the velocity of charged carriers is limited by the Fermi velocity ($v < v_F$), which is smaller than the graphene plasmon phase velocity ($v_F < v_p$), it seems impossible for the charged carriers in the graphene to excite Cherenkov-related graphene plasmon emission. However, involving interband transitions, the Cherenkov radiation can occur when the velocity is below the conventional threshold. The proposed mechanism also manifests an energy conversion efficiency as high as 78% from hot carriers to graphene plasmons.^[80]

4. Controlling Smith–Purcell Radiation by Metamaterials

4.1. Enhancement of the Radiation Intensity

In addition to the superradiant Smith–Purcell emission arising from the coherent interference, the radiation intensity can also be enhanced by the resonance effect. Several studies have

shown that for a metallic grating, the Smith–Purcell radiation can be enhanced at the resonant frequency of the grating.^[81–86] By designing the geometry parameter of the groove of the grating, we can adjust the resonance frequency of Smith–Purcell radiation. Coupling with the surface plasmon resonance is another approach to enhancing Smith–Purcell radiation.^[87–90] In the terahertz region, graphene is a unique platform for surface plasmons, which can be excited by moving charged particles^[91–93] and in turn enhance Smith–Purcell radiation. Zhan et al. studied the Smith–Purcell radiation for a dielectric grating covered by a single layer of graphene.^[93] The surface plasmon induced by the moving electrons could increase the terahertz radiation intensity up to ten orders of magnitude compared to the radiation from a dielectric grating. Recently, a theoretical work indicated that Smith–Purcell radiation can occur in aperiodic structures.^[94] Soon after, Kaminer et al. adopted an innovative experimental setup based on a scanning electron microscope to observe collective Smith–Purcell emission from the 2D plasmonic crystal with strong disorder.^[88] This setup could image the surface with a resolution of a few tens of nanometer and meanwhile detect the local radiation intensity. They fabricated samples of grating with line defects, as shown in **Figure 5a**, and measure the Smith–Purcell radiation of the defected samples. They observed in experiment an enhancement

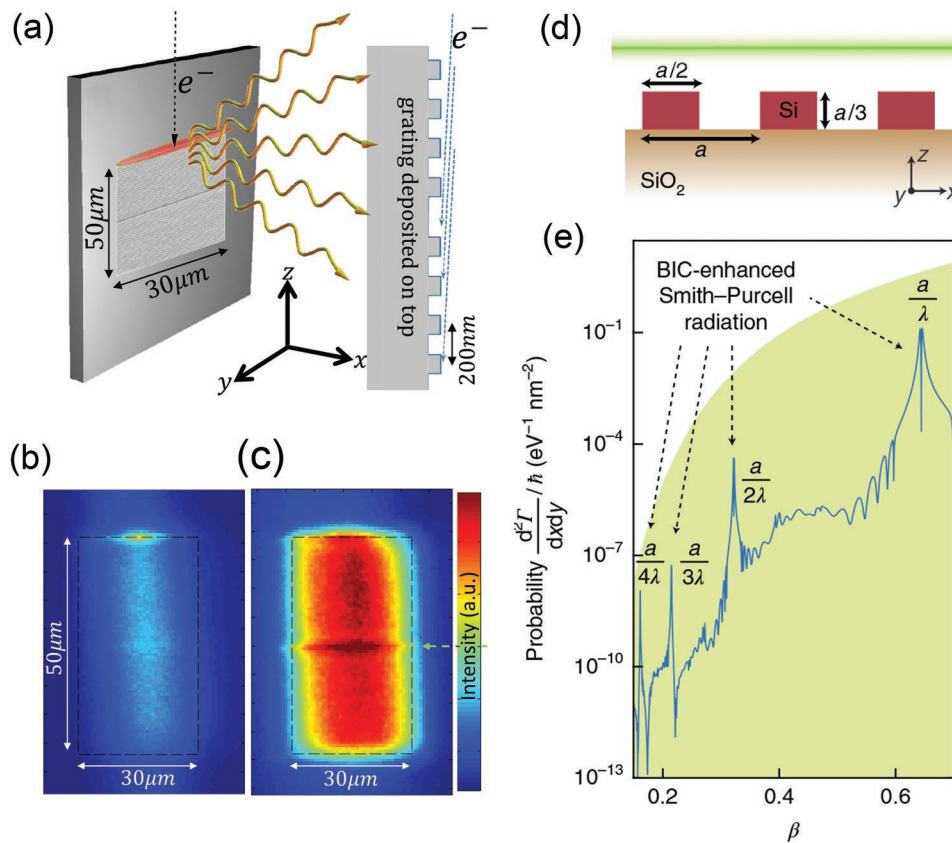


Figure 5. a) Illustration of an electron beam (dashed black arrow) interacting with line defects fabricated in the sample. b, c) Direct imaging of enhanced emission from the line defect. The kinetic energy of electrons is 13 and 20 kV in (b) and (c), respectively. d) Schematic drawing of an electron beam (green line) interacting with a silicon-on-insulator grating that is periodic along the x-axis and infinite along the y-axis. e) Emission probability at a given frequency for different electron velocities. Strong enhancement happens at electron velocities $\beta = a/m\lambda$ ($m = 1, 2, 3, \dots$). Shaded area corresponds to the theoretical limit of emission. (a)–(c) Reproduced with permission.^[89] Copyright 2017, American Physical Society. (d), (e) Reproduced with permission.^[95] Copyright 2018, Nature Publishing Group.

of Smith–Purcell radiation from the edge of the periodic part and the line defect of a silver grating, as shown in Figure 5b,c.

The maximum radiation energy of moving electrons near an arbitrary scatterer was investigated by Yang et al.^[95] Their results demonstrate that there are three key factors that determine maximal radiation: intrinsic material loss, particle velocity, and impact parameter defined as $k_p d$. Here d is the distance between

the moving particles and the structure, and $k_p = \sqrt{\left(\frac{\omega}{v}\right)^2 - k^2}$ (k is the free-space wave number). According to their calculation, if the moving particles are in the far field of the structure ($k_p d \gg 1$), stronger radiation intensity can be achieved by charged particles with higher velocity. By contrast, slower velocity is optimal in the case that the moving particles are in the near field ($k_p d \ll 1$), because slow electrons can generate stronger near-field amplitudes although the field is more evanescent. To find out the upper limit of radiation intensity, Yang et al. designed a 1D silicon grating (Figure 5d) to make the electron line intersect the TE₁ mode of the grating at the bound states in the continuum (BICs) by choosing appropriate electron velocities.^[95] The coupling between electrons and BICs enables the Smith–Purcell radiation to be enhanced by orders of magnitude, thanks to the high quality factor of BIC states.

The calculated emission probability of the dielectric grating at a given frequency is plotted in Figure 5e. It suggests that the BIC-enhancement mechanism agrees very well with the calculated upper limits of radiation.

4.2. Spatial Shaping of Smith–Purcell Radiation

Not only can the periodic structure increase the intensity of Smith–Purcell radiation, but also affect the spatial distribution of the radiation wave. The radiation spectrum can be controlled to exhibit multiple peaks by introducing complex periodicity and aperiodicity in the grating.^[96] It is because that the local change of the period will change the local phase of the radiation wave. Furthermore, the concept of “Smith–Purcell lens” has been proposed, which combined the source and lens together.^[96] By properly designing the period of the grating, the angle of the emitted radiation from each point on the grating can make the radiation match the phase profile of the lens for a specific emission wavelength. In the simulation, the intensity profile in the focal plane of the proposed lens exhibits a full width at half maximum above the diffraction limit. At another wavelength other than the designed wavelength, the lens will show a different focal length and lateral deflection. The proposed

Smith–Purcell lens has a strong chromatic dispersion due to the dispersive nature of Smith–Purcell radiation. Lai et al. have designed a Smith–Purcell lens working in visible range by an insulator–metal–insulator (IMI) structure.^[90] The frequency of Smith–Purcell radiation can be locked and enhanced at the frequency where the surface plasmons of the IMI structure are excited. By designing the period of the metal groove at the top layer of the IMI structure, a Smith–Purcell lens working at a single wavelength can be formed through the plasmon-locked Smith–Purcell radiation. The surface plasmons frequency of the IMI structure depends on the permittivity of the middle dielectric layer. The working frequency of the Smith–Purcell lens can also be changed when the permittivity of the middle dielectric layer is varied. By dividing the IMI substrate into three parts with different dielectric layer, the proposed Smith–Purcell lens could operate for blue, green, and red light.

4.3. Manipulating the Polarization

In conventional Smith–Purcell radiation using gratings, the radiated wave always exhibits transverse magnetic (TM) polarization, which is determined by the direction of dipole moments excited by the moving charged particles. However, in a recent letter, Wang et al. numerically demonstrated that polarization state of the electron-induced emission can be manipulated by the Babinet metasurface composed of C-aperture resonators, as shown in **Figure 6a**.^[97] For a metasurface composed of C-ring resonators, in-plane electric dipoles and out-plane magnetic dipoles can be excited. For its complementary structure (i.e., C-aperture resonators), the out-of-plane electric dipole and in-plane magnetic dipole can be induced because of the Babinet principle. By coupling the intrinsically nonradiative energy bound at the source current sheet to the in-plane magnetic dipole of the C-aperture resonator, the far-field radiation of cross polarization can be achieved due to the bianisotropic nature of the Babinet metasurface. Through changing the rotation angle α of the C-aperture resonator, the polarization angle β of the radiated light can be readily adjusted, and the polarization angle β simply equals the rotation angle α . The field distributions of Smith–Purcell radiation along the z -axis induced by the Babinet metasurface are depicted in **Figure 6b**.

We can find that the radiated light is purely TM wave when the orientation of the C-aperture resonator is $\alpha = 0^\circ$. In the case that the orientation is $\alpha = 90^\circ$, the transverse electric (TE) wave can be obtained. For comparison, the field distributions for Smith–Purcell radiation induced by the metasurface composed of C-ring resonators are presented in **Figure 6c**. Regardless of the orientation angle, the radiated light is TM polarized wave, because no electric dipoles along y -axis or magnetic dipoles along x -axis can be excited. It is noted that the radiated electric field is relatively weak for $\alpha = 0^\circ$ in **Figure 6c**. It is because that the orientation of the fundamental electric dipole mode of the C-ring resonator is orthogonal to the evanescent electric field of the moving charged particles.

5. Applications

Cherenkov radiation and Smith–Purcell emission manifest great potential in various applications especially for on-chip light sources and laser-driven electron accelerators. When combined with artificial structures such as metamaterials and photonic crystals, the performances of these devices can be greatly improved in the aspect of intensity, tunability, and compactness.

5.1. On-Chip Light Sources

Free-electron-driven sources, such as Smith–Purcell sources and Cherenkov sources, in which optical photons are emitted as an electron beam passes over the surface or travels through a metal/dielectric structure, offer a compactable and tunable platform to directly generate ultrabright and ultrabroadband light. Remarkably, the wavelength and direction of emitted light can be tuned from the microwave to ultraviolet region by adjusting the energy of the electron beam or the structure of the periodic surroundings. The free laser based on Cherenkov radiation and Smith–Purcell radiation has been proposed and fabricated.^[98–104] Artificially engineered metamaterials can tailor the interaction between the electron and matter, manifesting new opportunities to improve the sources' performance like radiation power density and other novel functionalities.

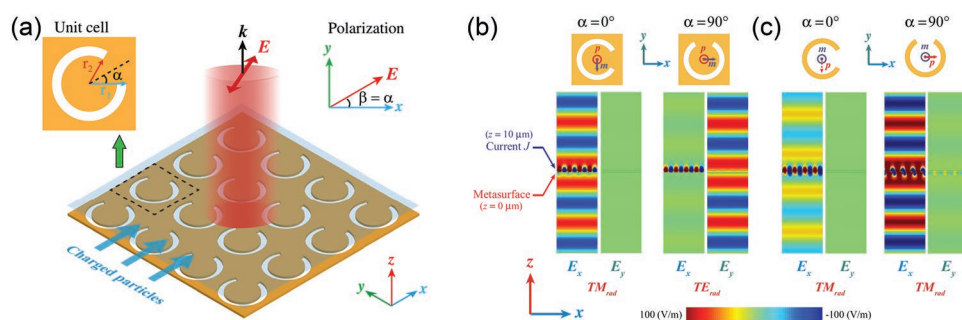


Figure 6. a) Schematic of the Smith–Purcell emission from a Babinet metasurface. A uniform sheet of charged particles moves closely parallel to the metasurface along the $+x$ axis. Linearly polarized radiation is generated, which propagates along the surface normal along the $+z$ direction. The polarization direction of the electric field is β with respect to the $+x$ axis, which is identical with the azimuthal rotating angle α of the C-aperture resonators. b,c) Simulated electric field distributions of the Smith–Purcell emission from b) C-aperture and c) C-ring metasurfaces for different rotation angles. (a)–(c) Reproduced with permission.^[97] Copyright 2016, American Physical Society.

Based on a multilayer metamaterial consisting of a periodically layered Au and SiO₂, Adamo et al. proposed a “Light Well” structure to provide the first proof-of-principle demonstration of a nanoscale, electron-beam-driven radiation source.^[79] As schematically shown in **Figure 7a**, an electron beam experiences a periodically modulated potential within the well, when it travels through a tunnel. Then light emission originates from an oscillating dipole induced by the electrons. Different from the classical Smith–Purcell effect, light emission occurs via coupling to the 1D photonic bands of the periodically structured well so that discrete emission wavelengths, determined by the wave vector of guided mode, are produced. However, the working efficiency is limited by surface plasmon generation and transverse light guiding, which only reaches an emission intensity of $\approx 200 \text{ W cm}^{-2}$. Later on, Liu et al. introduced a structure of nanometal film with dielectric-medium loading to enhance the Cherenkov radiation intensity as **Figure 7b** shows.^[105] By matching the Cherenkov radiation condition and the dispersion relation of surface plasmons, the transformation of surface plasmons into Cherenkov radiation is available as **Figure 7c** shows. The inset is the calculated emitted power spectrum for 100 keV. As the emission frequency is determined by the intersection of the beam line with the surface plasmon dispersion curve, in which the solution is only one point, the emission spectrum is quite narrow, thus the working efficiency has a prominent improvement at the peak. The radiation power density can reach or even exceed 10^8 W cm^{-2} . More importantly, Cherenkov radiation has a broad and continuous spectrum

in ordinary cases, and the maximum radiation frequency is dependent of the highest response frequency of the medium. However, in this work, radiation frequency is determined by the wave band of the waveguide and shows a narrow band property, which shows a potential for electron-driven laser.

Recently, graphene has emerged as a promising candidate for generation of high frequency radiation from relatively low-energy electrons, because it can support surface plasmons that exhibit extreme confinement of light with dynamic tunability by electrical gating.^[106,107] Wong et al. demonstrated that using electrons interacting with graphene plasmons, a highly directional, tunable, and monochromatic radiation source can be realized (**Figure 7d**).^[108] A sheet of graphene on a dielectric substrate sustains graphene plasmons, which can be excited by a focused laser beam illuminating on a grating structure. When electrons are launched parallel to the graphene sheet, their subsequent interaction with the strong field of graphene plasmons induces transverse electron oscillations, just like a quantum electron–photon interactions. However, because of the plasmon’s dispersion relation, electron–plasmon scattering spectrum is highly directional and monoenergetic, showing an on-axis full-width at half-maximum spread of only 0.25% and an angular spread of less than 10 mrad. In addition to controlling the kinetic energy of free electrons, the emitted light wavelength can also be tuned by tuning the frequency of the surface plasmon or by electrical gating to change the Fermi level of graphene, through which the emitted light wavelength can be tuned from infrared to X-ray regimes.

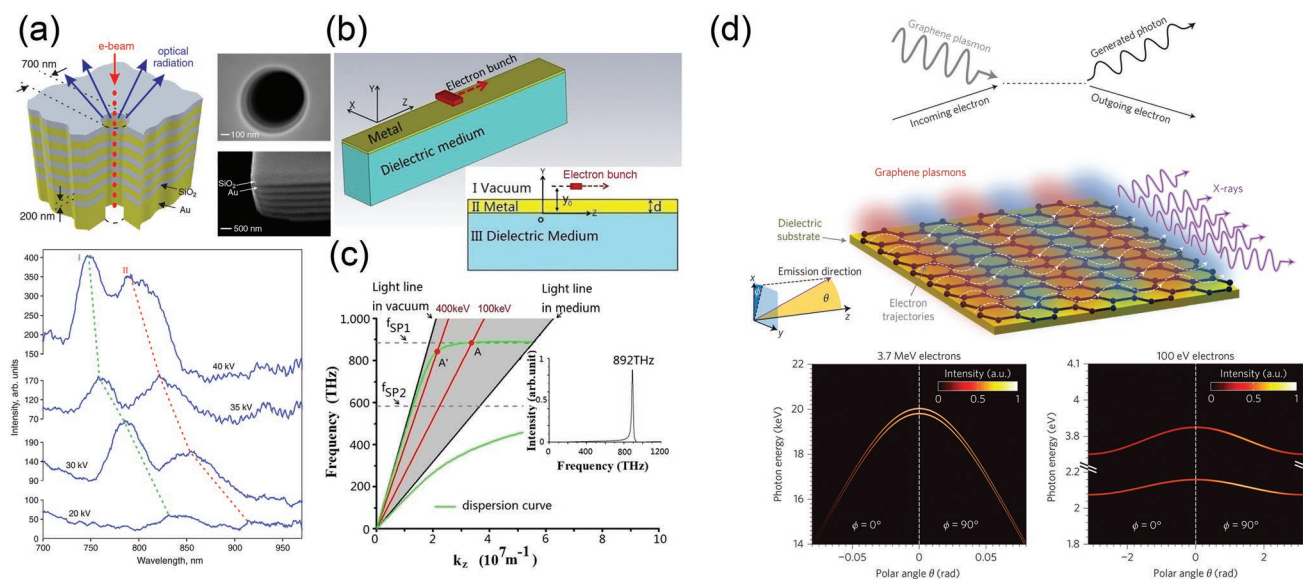


Figure 7. a) Top panel: schematic and scanning electron microscope image of a light well. The light well is a nanohole milled through a stack of alternating metal and dielectric layers. Bottom panel: the emission spectra for a well with diameter of 750 nm and acceleration voltages of 20, 30, 35, and 40 kV. b) Schematic of the planar structure surface plasmon Cherenkov light radiation source. Region I is vacuum, region II is a metal film, and region III is dielectric medium, respectively. c) Dispersion curves of 20 nm thick Ag film covering the dielectric medium. The intersection of the dispersion curves and electron beam lines of 100 and 400 keV electron energy lies at A and A'. f_{SP1} and f_{SP2} are the surface plasmon frequencies at the vacuum–metal and metal–dielectric interfaces, respectively. The inset shows the calculated power spectrum. d) Schematic showing the electron–plasmon interaction, in which free electrons (dotted white lines) interact with the graphene plasmon field (glowing red and blue bars) to produce short-wavelength output radiation. The resulting monochromatic radiation falls in the hard X-ray regime when modestly relativistic (3.7 MeV) electrons are used and in the visible/ultraviolet regime when nonrelativistic (100 eV) electrons are used. (a) Reproduced with permission.^[79] Copyright 2009, American Physical Society. (b),(c) Reproduced with permission.^[105] Copyright 2012, American Physical Society. (d) Reproduced with permission.^[108] Copyright 2016, Nature Publishing Group.

5.2. Laser-Driven Electron Accelerators

Modern particle accelerators use metallic cavities to confine electromagnetic modes with axial acceleration forces. The accelerating field is on the order $10\text{--}50\text{ MV m}^{-1}$, which is ultimately limited by the electrical breakdown of the metallic surfaces.^[109] To achieve ultra high-speed particles, the acceleration path for particles and thus the total length of the accelerator need to be large. Apparently, the larger the accelerator is, the more expensive it is. The state-of-the-art accelerators used for high energy physics usually have construction costs of the billions of dollars and occupy many square kilometers of area.^[110,111] Aiming to realize a compact and cost-effective accelerator, researchers have explored the use of lasers to accelerate charged particles since the invention of lasers in the early 1960s. The method proposed is called radiative processes in reverse, including the inverse Cherenkov accelerator^[112] and inverse Smith–Purcell accelerator.^[113,114] In this design,^[112] a cylindrical tube of maser material will be excited by pumping radiation through an interference filter, then an oscillation in a TM type mode will be generated. An optical peak power of 10 kW cm^{-2} was calculated to accelerate electrons by 10^9 eV m^{-1} . These proposals have been demonstrated experimentally with nonrelativistic electrons using a metallic grating at infrared wavelengths.^[115]

At the very beginning, structured metals were used for accelerating the electrons in the experiments.^[116] However, metallic surfaces suffer from high ohmic losses and low damage threshold limits at optical wavelengths. Due to these constraints, the research focus has been shifted toward photonic structures made of dielectric materials and incorporating new technologies such as photonic crystals and metasurfaces.^[117] A prominent example of the dielectric laser-based acceleration is shown in **Figure 8a**, in which the laser pulse is focused onto a fused silicon transmission grating and then excites the evanescent field to efficiently impart momentum on 28 keV electrons.^[117] **Figure 8b,c** shows the scanning electron microscope images of the dielectric grating and results of the electron acceleration, which demonstrates a maximum acceleration gradient of 25 MeV m^{-1} . This work is important in laying the ground work for efficient phased laser acceleration with a low-cost and compact properties.

Then a more complicated design has been proposed to realize a 250 MeV m^{-1} acceleration gradient, which is tenfold higher than the former work.^[118] The designed structure and experiment are shown in **Figure 8d,e**, respectively. By combining two opposite gratings to realize a multiple accelerating cavity, relativistic (60 MeV) electrons are energy-modulated over 563 ± 104 optical periods of a fused silica grating structure. By contrast, conventional modern linear accelerators operate at gradients of $10\text{--}30\text{ MeV m}^{-1}$, which means this design sets the stage for the development of future multi-staged dielectric laser accelerators devices composed of integrated on-chip systems. It would open a new paradigm for low-cost and table-top accelerators on the MeV–GeV scale for a wide range of applications, including security scanners and medical therapy, university-scale X-ray light sources for biological and materials research, and portable medical imaging devices.

6. Conclusions and Outlooks

After decades of development, the study on electron induced radiation is going broader and deeper. The applications of electron induced emission have been used in many fields, from electron microscope to medical imaging and therapy. Meanwhile, artificial photonic materials, including metamaterials, metasurfaces, plasmonic materials, and photonic crystals, have become prosperous in recent years, which allow us to tailor material properties on demand. Thanks to the development of artificial photonic materials, the study of the interaction between electrons and surrounding media has reached a new level. The combination of the two fields has enabled many extraordinary phenomena that were difficult or impossible to observe in conventional electron induced radiation. In turn, we have gained new insights into light–matter interaction at the nanoscale.

For Cherenkov radiation, the radiation direction and energy threshold can be significantly modified by artificial materials. Through changing the radiation angle of Cherenkov radiation, we can design Cherenkov detectors with higher sensitivity and much smaller size for the detection of high-energy particles. Thresholdless Cherenkov radiation paves a new way for novel radiation sources. The 2D Cherenkov radiation resulted from surface plasmons could be used as a compact nanoscale plasmon source. For Smith–Purcell radiation, the radiation intensity can be greatly enhanced by surface plasmon resonance or waveguide resonance mode of the metamaterial structure, which is very useful in designing highly efficient electron driven source. In addition, we have the capabilities of manipulating the polarization state of Smith–Purcell radiation by structured metasurfaces.

Although tremendous efforts have been made to investigate the interaction between the electrons and artificial structures, there are still many interesting topics worth further exploration. For instance, most previous works are limited to theoretically study and the experimental realization is still difficult, because it is challenging to apply a compact electron bunch on the metamaterial/metasurface. To verify the proposed new theories, we may apply some methods to mimic the electron bunch in the experiment. For example, SPP waves can be used as the source to replace the electron beams, since the field distributions of SPPs are analogous to the evanescent fields carried by charged particles when their velocity is low. In addition, the interaction between electrons and medium with specific permittivity distribution needs to be investigated. As we know, Cherenkov radiation depends on the effective refractive index of the surrounding medium. In addition to negative-index materials and hyperbolic metamaterials, the optical properties of other artificial materials have been proposed and studied, such as near-zero-index materials, parity-time symmetric metamaterials, and topological photonic materials. However, the interaction between electrons and these artificial materials has not been investigated, which is expected to induce new phenomena. Moreover, tunability of metamaterials is always of vital importance in the real-world applications. A lot of efforts have been devoted to realizing tunable metamaterials under external stimuli (e.g., external electric fields, magnetic fields, heat, and laser pulses).

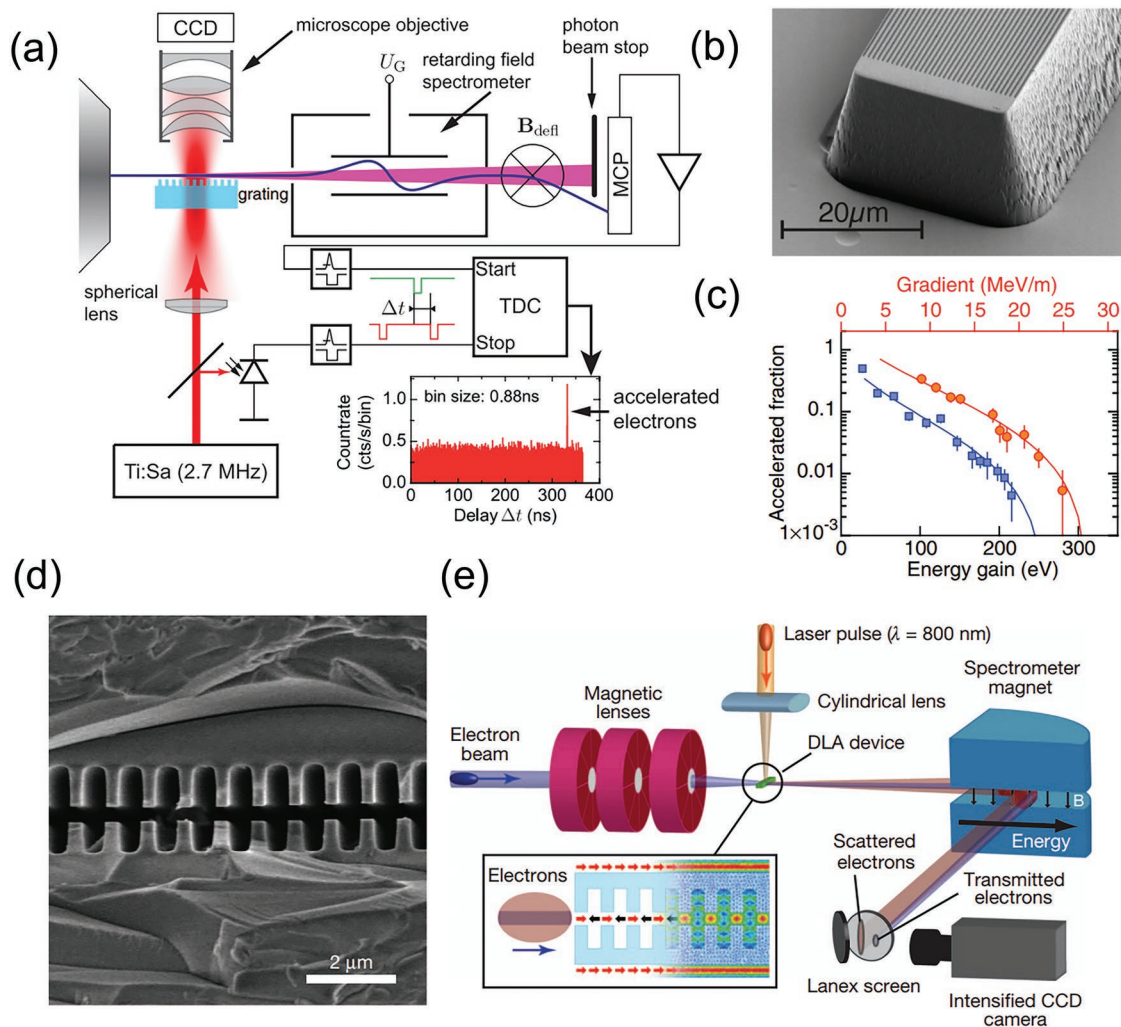


Figure 8. a) Sketch of the experimental setup and detection scheme. Electrons emitted from a scanning electron microscope column (left) pass the transparent grating, and interact with the accelerating field excited by the laser pulses that are illuminated from the bottom of the grating. A microscope objective is used to monitor the position of the laser focus. The electrons that can pass the spectrometer (center) are detected at the microchannel plate. The trajectories entering the spectrometer are drawn as slightly off center, causing the deviation from the electron optical axis inside the spectrometer. b) Scanning electron microscope image of a fused silica mesa structure used to demonstrate sub-relativistic acceleration with up to 25 MV m⁻¹ gradients. c) Electron acceleration results, showing the accelerated fraction of electrons as a function of energy gain (bottom axis) and acceleration gradient (top axis), for two different laser peak electric fields [$E_p = 2.85$ GV m⁻¹ (circles), $E_p = 2.36$ GV m⁻¹ (squares)]. The solid curves are simulation results. d) Scanning electron microscope image of the longitudinal cross-section of a dielectric laser accelerator structure. e) Experimental set-up. The inset shows a diagram of the dielectric laser accelerator structure, which indicates the field polarization direction and the effective periodic phase reset, depicted as alternating red (acceleration) and black (deceleration) arrows. A snapshot of the simulated fields in the structure shows the corresponding spatial modulation in the vacuum channel. (a)–(c) Reproduced with permission.^[17] Copyright 2013, American Physical Society. (d),(e) Reproduced with permission.^[18] Copyright 2013, Nature Publishing Group.

Combining tunable metamaterials with Cherenkov radiation and Smith–Purcell radiation can significantly expand their applications. Meanwhile, graphene not only has a tunable conductivity but also supports SPP resonances to tightly confine optical fields at the terahertz and infrared range. We can investigate Smith–Purcell radiation based on patterned graphene and potentially other 2D materials, which serve as the atomically thin platform.

To summarize, through artificially structured metamaterials and metasurfaces, electron induced radiation could exhibit many unprecedented physical phenomena, and lead to exciting applications with new functions, high efficiency, and small

device footprint. A lot of questions remain open in the area of the interaction between electrons and artificial materials. The research discoveries will provide us with many opportunities to advance the fundamental science and technological innovations in particle physics, astrophysics, engineering, and materials science.

Acknowledgements

R.P. was supported by the National Key R&D Program of China (Grant No. 2017YFA0303702) and the National Natural Science Foundation

of China (Grant Nos. 11634005 and 11621091). J.Y. acknowledges the support of National Natural Science Foundation of China (Grant No. 51572225).

Conflict of Interest

The authors declare no conflict of interest.

Keywords

Cherenkov radiation, electron-induced emission, metamaterials, metasurfaces, Smith–Purcell radiation

Received: November 30, 2018

Revised: March 5, 2019

Published online: April 1, 2019

-
- [1] F. J. García de Abajo, *Rev. Mod. Phys.* **2010**, *82*, 209.
 [2] A. P. Kobzev, *Phys. Part. Nucl.* **2014**, *45*, 628.
 [3] V. L. Ginsburg, *J. Exp. Theor. Phys.* **1946**, *16*, 15.
 [4] P. Goldsmith, J. V. Jelley, *Philos. Mag.* **1959**, *4*, 836.
 [5] P. A. Cherenkov, *Dokl. Akad. Nauk SSSR* **1934**, *2*, 451.
 [6] A. P. Potylitsyn, *Nucl. Instrum. Methods Phys. Res., Sect. B* **1998**, *145*, 169.
 [7] S. J. Smith, E. M. Purcell, *Phys. Rev.* **1953**, *92*, 1069.
 [8] D. Y. Sergeeva, A. A. Tishchenko, M. N. Strikhanov, *Phys. Rev. Spec. Top.—Accel. Beams* **2015**, *18*, 052801.
 [9] T. M. Shaffer, E. C. Pratt, J. Grimm, *Nat. Nanotechnol.* **2017**, *12*, 106.
 [10] D. Smith, J. Pendry, M. Wiltshire, *Science* **2004**, *305*, 788.
 [11] C. M. Soukoulis, M. Wegener, *Nat. Photonics* **2011**, *5*, 523.
 [12] Y. Liu, X. Zhang, *Chem. Soc. Rev.* **2011**, *40*, 2494.
 [13] W. Cai, V. M. Shalaev, *Optical Metamaterials: Fundamentals and Applications*, Springer-Verlag, New York **2010**.
 [14] D. R. Smith, N. Kroll, *Phys. Rev. Lett.* **2000**, *85*, 2933.
 [15] J. Valentine, S. Zhang, T. Zentgraf, E. Ulin-Avila, D. A. Genov, G. Bartal, X. Zhang, *Nature* **2008**, *455*, 376.
 [16] V. Mocella, S. Cabrini, A. Chang, P. Dardano, L. Moretti, I. Rendina, D. Olynick, B. Harteneck, S. Dhuey, *Phys. Rev. Lett.* **2009**, *102*, 133902.
 [17] E. J. R. Vespeur, T. Coenen, H. Caglayan, N. Engheta, A. Polman, *Phys. Rev. Lett.* **2013**, *110*, 013902.
 [18] J.-T. Shen, P. B. Catrysse, S. Fan, *Phys. Rev. Lett.* **2005**, *94*, 197401.
 [19] M. Choi, S. H. Lee, Y. Kim, S. B. Kang, J. Shin, M. H. Kwak, K. Y. Kang, Y. H. Lee, N. Park, B. Min, *Nature* **2011**, *470*, 369.
 [20] J. Hao, Y. Yuan, L. Ran, T. Jiang, J. A. Kong, C. Chan, L. Zhou, *Phys. Rev. Lett.* **2007**, *99*, 063908.
 [21] A. Poddubny, I. Iorsh, P. Belov, Y. Kivshar, *Nat. Photonics* **2013**, *7*, 948.
 [22] J. K. Gansel, M. Thiel, M. S. Rill, M. Decker, K. Bade, V. Saile, G. von Freymann, S. Linden, M. Wegener, *Science* **2009**, *325*, 1513.
 [23] A. Kuzyk, R. Schreiber, Z. Fan, G. Pardatscher, E.-M. Roller, A. Högele, F. C. Simmel, A. O. Govorov, T. Liedl, *Nature* **2012**, *483*, 311.
 [24] Y. Zhao, M. Belkin, A. Alù, *Nat. Commun.* **2012**, *3*, 870.
 [25] S.-C. Jiang, X. Xiong, Y.-S. Hu, Y.-H. Hu, G.-B. Ma, R.-W. Peng, C. Sun, M. Wang, *Phys. Rev. X* **2014**, *4*, 021026.
 [26] N. Segal, S. Keren-Zur, N. Hendler, T. Ellenbogen, *Nat. Photonics* **2015**, *9*, 180.
 [27] G. A. Wurtz, R. Pollard, W. Hendren, G. P. Wiederrecht, D. J. Gosztola, V. A. Podolskiy, A. V. Zayats, *Nat. Nanotechnol.* **2011**, *6*, 107.
 [28] J. Lee, M. Tymchenko, C. Argyropoulos, P.-Y. Chen, F. Lu, F. Demmerle, G. Boehm, M.-C. Amann, A. Alù, M. A. Belkin, *Nature* **2014**, *511*, 65.
 [29] J. B. Pendry, *Phys. Rev. Lett.* **2000**, *85*, 3966.
 [30] N. Fang, H. Lee, C. Sun, X. Zhang, *Science* **2005**, *308*, 534.
 [31] Z. Liu, H. Lee, Y. Xiong, C. Sun, X. Zhang, *Science* **2007**, *315*, 1686.
 [32] J. B. Pendry, D. Schurig, D. R. Smith, *Science* **2006**, *312*, 1780.
 [33] U. Leonhardt, *Science* **2006**, *312*, 1777.
 [34] A. Alù, N. Engheta, *Phys. Rev. E* **2005**, *72*, 016623.
 [35] H. Chen, C. Chan, P. Sheng, *Nat. Mater.* **2010**, *9*, 387.
 [36] Y. Liu, X. Zhang, *Nanoscale* **2012**, *4*, 5277.
 [37] A. V. Kildishev, A. Boltasseva, V. M. Shalaev, *Science* **2013**, *339*, 1232009.
 [38] N. F. Yu, F. Capasso, *Nat. Mater.* **2014**, *13*, 139.
 [39] H.-T. Chen, A. J. Taylor, N. Yu, *Rep. Prog. Phys.* **2016**, *79*, 076401.
 [40] X. Luo, *Adv. Opt. Mater.* **2018**, *6*, 1701201.
 [41] N. F. Yu, P. Genevet, M. A. Kats, F. Aieta, J. P. Tetienne, F. Capasso, Z. Gaburro, *Science* **2011**, *334*, 333.
 [42] X. Ni, N. K. Emani, A. V. Kildishev, A. Boltasseva, V. M. Shalaev, *Science* **2012**, *335*, 427.
 [43] L. L. Huang, X. Z. Chen, H. Mühlenbernd, G. X. Li, B. F. Bai, Q. F. Tan, G. F. Jin, T. Zentgraf, S. Zhang, *Nano Lett.* **2012**, *12*, 5750.
 [44] C. Pfeiffer, A. Grbic, *Phys. Rev. Lett.* **2013**, *110*, 197401.
 [45] L. X. Liu, X. Q. Zhang, M. Kenney, X. Q. Su, N. N. Xu, C. M. Ouyang, Y. L. Shi, J. G. Han, W. L. Zhang, S. Zhang, *Adv. Mater.* **2014**, *26*, 5031.
 [46] Y. Yang, W. Wang, P. Moitra, I. I. Kravchenko, D. P. Briggs, J. Valentine, *Nano Lett.* **2014**, *14*, 1394.
 [47] D. Lin, P. Fan, E. Hasman, M. L. Brongersma, *Science* **2014**, *345*, 298.
 [48] G. Zheng, H. Mühlenbernd, M. Kenney, G. Li, T. Zentgraf, S. Zhang, *Nat. Nanotechnol.* **2015**, *10*, 308.
 [49] A. Arbabi, Y. Horie, M. Bagheri, A. Faraon, *Nat. Nanotechnol.* **2015**, *10*, 937.
 [50] S. M. Wang, P. C. Wu, V. C. Su, Y. C. Lai, C. H. Chu, J. W. Chen, S. H. Lu, J. Chen, B. B. Xu, C. H. Kuan, T. Li, S. N. Zhu, D. P. Tsai, *Nat. Commun.* **2017**, *8*, 187.
 [51] S.-C. Jiang, X. Xiong, Y.-S. Hu, S.-W. Jiang, Y.-H. Hu, D.-H. Xu, R.-W. Peng, M. Wang, *Phys. Rev. B* **2015**, *91*, 125421.
 [52] I. Tamm, I. Frank, *Dokl. Akad. Nauk SSSR* **1937**, *14*, 109.
 [53] A. P. Kobzev, *Phys. Part. Nucl.* **2010**, *41*, 452.
 [54] P. M. van den Berg, *J. Opt. Soc. Am.* **1973**, *63*, 689.
 [55] P. M. van den Berg, *J. Opt. Soc. Am.* **1973**, *63*, 1588.
 [56] P. M. van den Berg, T. H. Tan, *J. Opt. Soc. Am.* **1974**, *64*, 325.
 [57] K. Ishii, Y. Shibata, T. Takahashi, S. Hasebe, M. Ikezawa, K. Takami, T. Matsuyama, K. Kobayashi, Y. Fujita, *Phys. Rev. E* **1995**, *51*, R5212.
 [58] K. J. Woods, J. E. Walsh, R. E. Stoner, H. G. Kirk, R. C. Fernow, *Phys. Rev. Lett.* **1995**, *74*, 3808.
 [59] J. Urata, M. Goldstein, M. F. Kimmitt, A. Naumov, C. Platt, J. E. Walsh, *Phys. Rev. Lett.* **1998**, *80*, 516.
 [60] H. L. Andrews, C. H. Boulware, C. A. Brau, J. D. Jarvis, *Phys. Rev. Spec. Top.—Accel. Beams* **2005**, *8*, 050703.
 [61] A. Gover, *Phys. Rev. Spec. Top.—Accel. Beams* **2005**, *8*, 030701.
 [62] G. V. Viktor, *Phys.-Usp.* **1968**, *10*, 509.
 [63] J. Lu, T. M. Grzegorzczuk, Y. Zhang, J. Pacheco, B. I. Wu, J. A. Kong, M. Chen, *Opt. Express* **2003**, *11*, 723.
 [64] H. Chen, M. Chen, *Mater. Today* **2011**, *14*, 34.
 [65] Z. Duan, B. I. Wu, J. Lu, J. A. Kong, M. Chen, *Opt. Express* **2008**, *16*, 18479.
 [66] Z. Duan, B.-I. Wu, J. Lu, J. Au Kong, M. Chen, *J. Appl. Phys.* **2008**, *104*, 063303.
 [67] S. Xi, H. Chen, T. Jiang, L. Ran, J. Huangfu, B.-I. Wu, J. A. Kong, M. Chen, *Phys. Rev. Lett.* **2009**, *103*, 194801.

- [68] Z. Duan, X. Tang, Z. Wang, Y. Zhang, X. Chen, M. Chen, Y. Gong, *Nat. Commun.* **2017**, *8*, 14901.
- [69] V. Ginis, J. Danckaert, I. Veretennicoff, P. Tassin, *Phys. Rev. Lett.* **2014**, *113*, 167402.
- [70] X. Lin, S. Easo, Y. Shen, H. Chen, B. Zhang, J. D. Joannopoulos, M. Soljačić, I. Kaminer, *Nat. Phys.* **2018**, *14*, 816.
- [71] P. Genevet, D. Wintz, A. Ambrosio, A. She, R. Blanchard, F. Capasso, *Nat. Nanotechnol.* **2015**, *10*, 804.
- [72] T. E. Stevens, J. K. Wahlstrand, J. Kuhl, R. Merlin, *Science* **2001**, *291*, 627.
- [73] C. Luo, M. Ibanescu, S. G. Johnson, J. D. Joannopoulos, *Science* **2003**, *299*, 368.
- [74] D. E. Fernandes, S. I. Maslovski, M. G. Silveirinha, *Phys. Rev. B* **2012**, *85*, 155107.
- [75] V. V. Vorobev, A. V. Tyukhtin, *Phys. Rev. Lett.* **2012**, *108*, 184801.
- [76] J.-K. So, J.-H. Won, M. A. Sattarov, S.-H. Bak, K.-H. Jang, G.-S. Park, D. S. Kim, F. J. Garcia-Vidal, *Appl. Phys. Lett.* **2010**, *97*, 151107.
- [77] A. Bera, R. K. Barik, M. Sattarov, O. Kwon, S. H. Min, I. K. Baek, S. Kim, J. K. So, G. S. Park, *Opt. Express* **2014**, *22*, 3039.
- [78] F. Liu, L. Xiao, Y. Ye, M. Wang, K. Cui, X. Feng, W. Zhang, Y. Huang, *Nat. Photonics* **2017**, *11*, 289.
- [79] G. Adamo, K. F. MacDonald, Y. H. Fu, C. M. Wang, D. P. Tsai, F. J. de Abajo, N. I. Zheludev, *Phys. Rev. Lett.* **2009**, *103*, 113901.
- [80] I. Kaminer, Y. T. Katan, H. Buljan, Y. Shen, O. Ilic, J. J. López, L. J. Wong, J. D. Joannopoulos, M. Soljačić, *Nat. Commun.* **2016**, *7*, 11880.
- [81] W. Liu, Z. Xu, *New J. Phys.* **2014**, *16*, 073006.
- [82] W. Liu, W. Li, Z. He, Q. Jia, *AIP Adv.* **2015**, *5*, 127135.
- [83] P. Zhang, Y. Zhang, M. Tang, *Opt. Express* **2017**, *25*, 10901.
- [84] L. Liang, W. Liu, Y. Liu, Q. Jia, L. Wang, Y. Lu, *Appl. Phys. Lett.* **2018**, *113*, 013501.
- [85] Y. Song, J. Du, N. Jiang, L. Liu, X. Hu, *Opt. Lett.* **2018**, *43*, 4590.
- [86] T. Zhao, M. Hu, Z. Lian, R. Zhong, S. Gong, C. Zhang, S. Liu, *Appl. Phys. Express* **2018**, *11*, 082801.
- [87] W. Liu, *Opt. Lett.* **2015**, *40*, 4579.
- [88] B. H. Cheng, Y. S. Ye, Y. C. Lan, D. P. Tsai, *Sci. Rep.* **2017**, *7*, 6443.
- [89] I. Kaminer, S. E. Kooi, R. Shiloh, B. Zhen, Y. Shen, J. J. López, R. Remez, S. A. Skirlo, Y. Yang, J. D. Joannopoulos, A. Arie, M. Soljačić, *Phys. Rev. X* **2017**, *7*, 011003.
- [90] Y. C. Lai, T. C. Kuang, B. H. Cheng, Y. C. Lan, D. P. Tsai, *Sci. Rep.* **2017**, *7*, 11096.
- [91] S. A. Mikhailov, *Phys. Rev. B* **2013**, *87*, 115405.
- [92] K. Tantiwanichapan, X. Wang, A. K. Swan, R. Paiella, *Appl. Phys. Lett.* **2014**, *105*, 241102.
- [93] T. Zhan, D. Han, X. Hu, X. Liu, S.-T. Chui, J. Zi, *Phys. Rev. B* **2014**, *89*, 245434.
- [94] J. R. M. Saavedra, D. Castells-Graells, F. J. García de Abajo, *Phys. Rev. B* **2016**, *94*, 035418.
- [95] Y. Yang, A. Massuda, C. Roques-Carnes, S. E. Kooi, T. Christensen, S. G. Johnson, J. D. Joannopoulos, O. D. Miller, I. Kaminer, M. Soljačić, *Nat. Phys.* **2018**, *14*, 894.
- [96] R. Remez, N. Shapira, C. Roques-Carnes, R. Tirele, Y. Yang, Y. Lereah, M. Soljačić, I. Kaminer, A. Arie, *Phys. Rev. A* **2017**, *96*, 061801(R).
- [97] Z. Wang, K. Yao, M. Chen, H. Chen, Y. Liu, *Phys. Rev. Lett.* **2016**, *117*, 157401.
- [98] V. Brasch, M. Geiselmann, T. Herr, G. Lihachev, M. H. P. Pfeiffer, M. N. Korodetsky, T. J. Kippenberg, *Science* **2016**, *351*, 357.
- [99] K. Suizu, K. Koketsu, T. Shibuya, T. Tsutsui, T. Akiba, K. Kawase, *Opt. Express* **2009**, *17*, 6676.
- [100] D. H. Auston, K. P. Cheung, J. A. Valdmanis, D. A. Kleinman, *Phys. Rev. Lett.* **1984**, *53*, 1555.
- [101] J. Gardelle, P. Modin, J. T. Donohue, *IEEE Trans. Terahertz Sci. Technol.* **2017**, *7*, 151.
- [102] D. N. Klochkov, K. B. Oganessian, E. A. Ayyan, N. S. Izmailian, *J. Mod. Opt.* **2016**, *63*, 653.
- [103] L. Schächter, A. Ron, *Phys. Rev. A* **1989**, *40*, 876.
- [104] C. Prokop, P. Piot, M. C. Lin, P. Stoltz, *Appl. Phys. Lett.* **2010**, *96*, 151502.
- [105] S. Liu, P. Zhang, W. Liu, S. Gong, R. Zhong, Y. Zhang, M. Hu, *Phys. Rev. Lett.* **2012**, *109*, 153902.
- [106] A. N. Grigorenko, M. Polini, K. S. Novoselov, *Nat. Photonics* **2012**, *6*, 749.
- [107] T. Low, P. Avouris, *ACS Nano* **2014**, *8*, 1086.
- [108] L. J. Wong, I. Kaminer, O. Ilic, J. D. Joannopoulos, M. Soljačić, *Nat. Photonics* **2016**, *10*, 46.
- [109] A. Grudiev, S. Calatroni, W. Wuensch, *Phys. Rev. Spec. Top.—Accel. Beams* **2009**, *12*, 102001.
- [110] Argonne National Lab. (ANL), Argonne, IL (United States); Pacific Northwest National Lab. (PNNL), Richland, WA (United States); SLAC National Accelerator Lab., Menlo Park, CA (United States); Fermi National Accelerator Lab. (FNAL), Batavia, IL (United States).
- [111] ILC Collaboration (T. Behnke et al.), *The International Linear Collider Technical Design Report*, ILC-REPORT-2013-040, May **2013**.
- [112] K. Shimoda, *Appl. Opt.* **1962**, *1*, 33.
- [113] Y. Takeda, I. Matsui, *Nucl. Instrum. Methods* **1968**, *62*, 306.
- [114] R. B. Palmer, presented at *11th Int. Conf. High-Energy Accelerators*, Geneva, Switzerland, July **1980**.
- [115] K. Mizuno, J. Pae, T. Nozokido, K. Furuya, *Nature* **1987**, *328*, 45.
- [116] C. M. S. Sears, E. Colby, R. J. England, R. Ischebeck, C. McGuinness, J. Nelson, R. Noble, R. H. Siemann, J. Spencer, D. Walz, T. Plettner, R. L. Byer, *Phys. Rev. Spec. Top.—Accel. Beams* **2008**, *11*, 101301.
- [117] J. Breuer, P. Hommelhoff, *Phys. Rev. Lett.* **2013**, *111*, 134803.
- [118] E. A. Peralta, K. Soong, R. J. England, E. R. Colby, Z. Wu, B. Montazeri, C. McGuinness, J. McNeur, K. J. Leedle, D. Walz, E. B. Sozer, B. Cowan, B. Schwartz, G. Travish, R. L. Byer, *Nature* **2013**, *503*, 91.